(Received 13 April 2024, Accepted 27 June 2024, Scheduled 8 July 2024)

Gradient Indexed Porous Core Photonic Crystal Fiber for Sub-Wavelength Confinement in Terahertz Regime

Kandaswamy Renuka Rani[1], Natesan Yogesh[2], and Krishnan Chitra[3,*]

[1]School of Advanced Sciences, Vellore Institute of Technology, Vandalur-Kelambakkam Road, Chennai, Tamil Nadu-600 127, India
[2]Department of Physics, National Institute of Technology Calicut, Kozhikode-673601, Kerala, India
[3]School of Electronics Engineering, Vellore Institute of Technology, Vandalur-Kelambakkam Road
Chennai, Tamil Nadu-600 127, India

ABSTRACT: A gradient-indexed core photonic crystal fiber (PCF) is proposed to realize sub-wavelength field confinement in the terahertz (THz) regime. It is verified that the gradient index (GRIN) profile PCF confirms superior field localization compared to the standard PCF. The in-plane quality factor of the GRIN PCF is evaluated as 2.2849×10^9 which is 10 times greater than the conventional case. Moreover, the power fraction is found to be 84.04% and 99.69% along with the confinement loss of 0.31 dB/cm and 0.341×10^{-7} dB/cm for the standard and GRIN type PCF at 0.2 THz. It is significant that the designed PCF also produces radial and azimuthal polarizations with enhanced field propagation due to the implicated triangular GRIN profile. The proposed GRIN PCF is useful for sub-THz communication, sensing and imaging applications.

1. INTRODUCTION

Photonic crystals (PhCs) are enviable optical structures for manipulating light flow [1]. The 2-D periodic PhCs are accessible in the form of Photonic crystal fibers (PCFs), a special type of microstructured fiber called holey fiber comprised of an array of air holes in a dielectric medium. PCF is an illustration of a 2-D PhC arrangement where light propagation is nearly at right angles to the plane. The holey fiber has stimulated an enduring research interest in the domains of telecommunication [2], astronomy [3], metrology [4], spectroscopy [5], lasers [6], amplifiers [7], and sensors [8–10]. The guiding mechanisms exploited within hollow-core [11] and porous or solid-core [12] PCF are (i) Photonic bandgap [13] (a range of electromagnetic frequencies not allowed to propagate through the photonic crystal) and (ii) index-guiding (light passing from denser to rarer medium is internally reflected and results in the effective confinement of light). Consequently, the exceptional optical characteristics of PCFs put forward an inclusive potential to affect the core-clad refractive index contrast owed to the air-holes configuration. Thus, PCF transcends the standard optical fiber as it possesses various admirable properties such as effective mode area, power fraction, dispersion, and confinement loss.

Among the research community, the concept of GRIN profile is introduced in the PhC assembly for the applications namely spatial beam compression [14], imaging [15, 16], coupler [17], mode conversion [18], sensing [19], waveguide bends [20], collimator [21], slow-light generation [22], supercontinuum generation [23], transmission of orbital angular momentum (OAM) modes [24], and delay line [25]. The reported research works on the sub-wavelength confinement are as follows: A PhC microcavity is proposed to attain field distribution of the configuration etched within a silicon-on-insulator waveguide [26] and a PhC micro-cavity to examine the effect of a near-field probe on the confined optical modes [27]. Micro- and nano-dielectric waveguide structures are employed for the realization of sub-wavelength optical beams [28], and sub-wavelength probing is studied using PhC nano-cavities [29]. Experimental demonstration of a dielectric bow-tie PhC structure assists mode volumes and quality factors with ultralow losses [30]. An efficient mode converter is established to interface a deep-sub-wavelength structure together with a PhC waveguide platform [31]. A hybrid Bloch surface polariton waveguide structure consisting of a dielectric nanowire located on a 1-D PhC multilayer dielectric stack reveals sub-wavelength light transportation with ultra-low propagation loss [32]. A split ring-shaped PhC unit cell maintains low loss and sub-wavelength localization of electric field in air [33]. A graphene plasmonic waveguide [34] and a hybrid optical waveguide comprising a dielectric nanowire detached from a metal surface employing a nanoscale dielectric gap are analyzed for long-range propagation [35].

In the proposed work, the employment of a triangular GRIN profile in the porous core of the PCF is newly attempted for the sub-wavelength confinement. The PhCs with metallic and dielectric structures were studied for sub-wavelength confinement previously. In our work, a triangular GRIN profile porous core PCF is introduced for sub-wavelength confinement with extreme light concentration. In addition to this sub-wavelength confinement, the modelled GRIN PCF supports various modes compared to the conventional PCF including radially and azimuthally polarized OAM modes [36–41]. The OAM modes

* Corresponding author: Krishnan Chitra (chitra.krishnan@vit.ac.in).

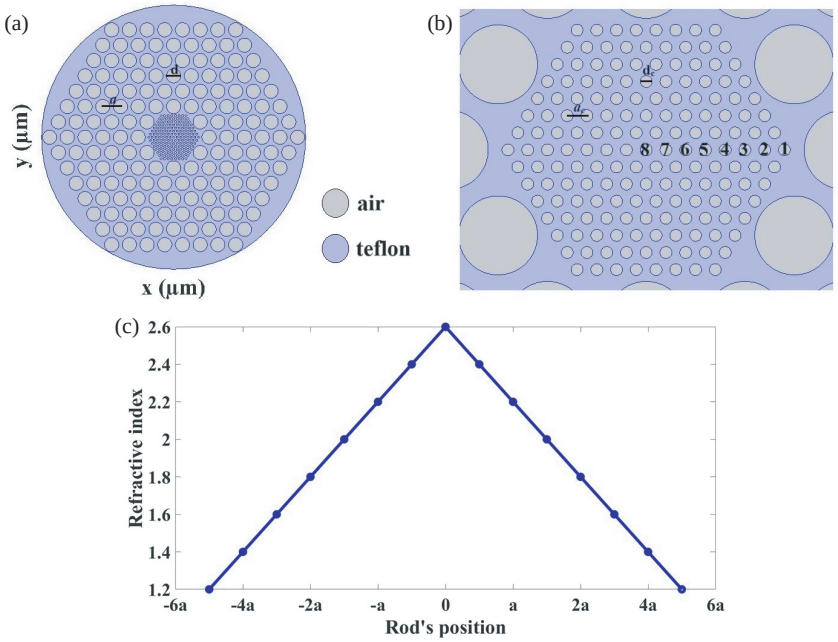


FIGURE 1. (a) 2-D PCF geometry with $a = 1000$ µm and $r = 0.4a$, (b) porous core with $a_c = 200$ µm and $r_c = 0.06a$ (enlarged view) showing GRIN profile in the porous core from 8 to 1, (c) Refractive index variation for different rod's positions.

of the GRIN PhCs are useful in plasmon excitation, high-resolution microscopy, material processing, optical confinement, acceleration of electrons, laser machining, and topology.

Additionally, the suggested triangular GRIN profile establishes effective light confinement by averting the escape of the field towards the cladding. We demonstrate the proposed design of GRIN PCF at terahertz (THz) frequencies. In recent years, THz wave has transfigured the entire world by its non-ionizing trait and developed into a prominently consumed electromagnetic (EM) radiation meant for guiding purposes [42]. Henceforth, the THz source from 0.15 THz to 0.2 THz is chosen for the investigation of GRIN PCF as this range affords better possibilities. In the computational process, the resonant modes with higher quality factors and lower confinement loss have been achieved for communication and imaging at the THz waveband.

2. DESIGN OF TRIANGULAR GRIN PCF

The geometry of the PCF entails a hexagonal lattice containing six layers of air holes of radius, $r = 0.4a$ (where clad air holes diameter, $d = 0.8a$) with lattice constant, $a = 1000$ µm, and the core of the PCF is made up of seven layers of tiny pores of radius, $r_c = 0.06a$ (where core air holes diameter, $d_c = 0.12a$) with lattice spacing $a_c = 200$ µm. The fiber material is considered Teflon due to its excellent properties in the THz regime. The modelled PCF is shown in Fig. 1(a) with the enlarged image of the microstructured core in Fig. 1(b) and a triangular GRIN fit in Fig. 1(c) for different rod's positions.

A triangular GRIN profile is implemented in the porous core of the proposed PCF where 'n' linearly varies in the radial direction as per the choice of gradient index coefficient α in the triangular GRIN profile. This refractive index contrast in the porous core alters the spatial distribution of the modes and brings about a shift in the resonant frequency of GRIN PCF compared to the normal PCF. The computed refractive indices are tailored with the triangular index profile presented by the following equation [14],

$$n(r) = n_0 \left(1 - \frac{\alpha}{2} |r|\right) \tag{1}$$

where $n(r)$ is the position-dependent refractive index, n_0 the refractive index of the center rod, and α the gradient coefficient of the realized triangular index profile which is easier to fabricate compared to the parabolic index profile. To achieve sub-wavelength field confinement, a triangular GRIN profile is presented in the porous core of the PCF. This particular GRIN profile is used as per the PCF's triangular lattice geometry, and this refractive index profile is not similar in the porous core. It is maximum at the centre and steadily decreases till it coincides with the cladding (as indicated from 8 to 1 in Fig. 1(b)). Here, the GRIN difference of 0.2 is chosen between the adjacent core layers, and this steady change in the index lowers modal dispersion.

3. CONFINEMENT AND PROPAGATION CHARACTERISTICS

The confinement of THz wave is examined using finite-element method (FEM) based COMSOL Multiphysics RF Module by solving the geometry through eigenmode analysis. The electric field map displayed in Figs. 2(a)–(d) distinguishes the localization of HE_{11} mode amid normal and GRIN type PCF which is accompanied by the respective 3-D view for auxiliary

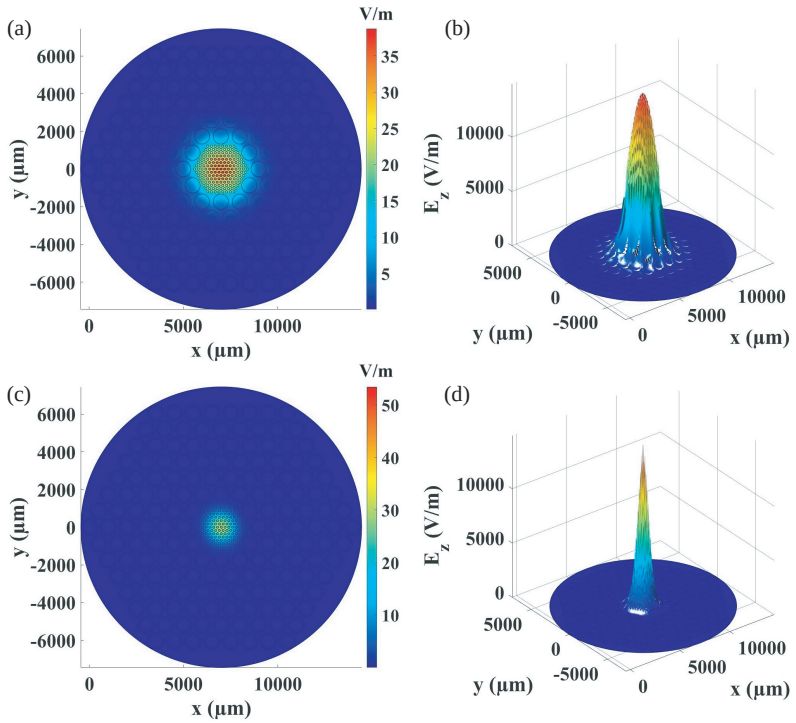


FIGURE 2. The electric field pattern of HE_{11} mode at 0.2 THz with a 3-D view, (a)–(b) normal type PCF, (c)–(d) GRIN type PCF.

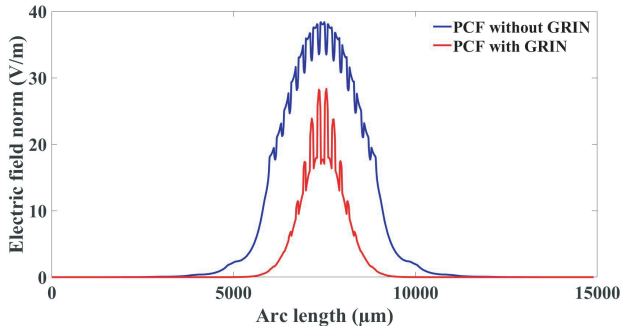


FIGURE 3. Illustration of sub-wavelength confinement using GRIN PCF at 0.2 THz. Here the arc length represents the measure of the distance along the curved line making up the arc and it is longer than the straight-line distance between its endpoints. Here, we produced the transverse or horizontal section of the PCF geometry (x-axis) from 0 to 15000 µm as the arc length.

elucidation. It can be verified that the light confinement becomes more intense when the GRIN profile comes into the picture of the modelled PCF. Fig. 3 illustrates the subwavelength confinement at 0.2 THz delivering a sharp intense beam due to the GRIN profile. The spatial full-width at half-maximum (FWHM) for normal and GRIN type PCFs is calculated as 1.7546λ and 0.6417λ which authenticates sub-wavelength field localization of the proposed GRIN PCF.

Certain eigenmodes signify radial and azimuthal polarizations with OAM as shown in Figs. 4(a)–(h) for normal and GRIN PCFs at 0.2 THz. By comparing these radially and azimuthally polarized modes, it was found that the improved localization of light is observed for GRIN PCF. Furthermore, the number of modes per unit volume per unit energy is higher for the GRIN profile as it produces supplementary OAM modes as depicted in Figs. 5(a)–(j) compared to normal profile PCF.

The propagation of the THz wave is explored using a Finite-Integration-Method-based CST Studio Suite EM solver as shown in Figs. 6(a)–(b) with a 3-D view in Figs. 6(c)–(d). From this figure, it is evident that the propagation spreads over the cladding for the standard PCF together with back reflection, but in the case of GRIN PCF, confined propagation is observed at 0.2 THz.

During the simulation of PCF, probes are placed at a distance of 0.2 cm along the length of the PCF, and the field is monitored from 0.15 THz to 0.2 THz as seen in Fig. 7. In normal PCF, the incident wave travels forward initially and later on shifts backward indicating reflection through the incident port. In contrast, the incident wave propagates in the forward direction and

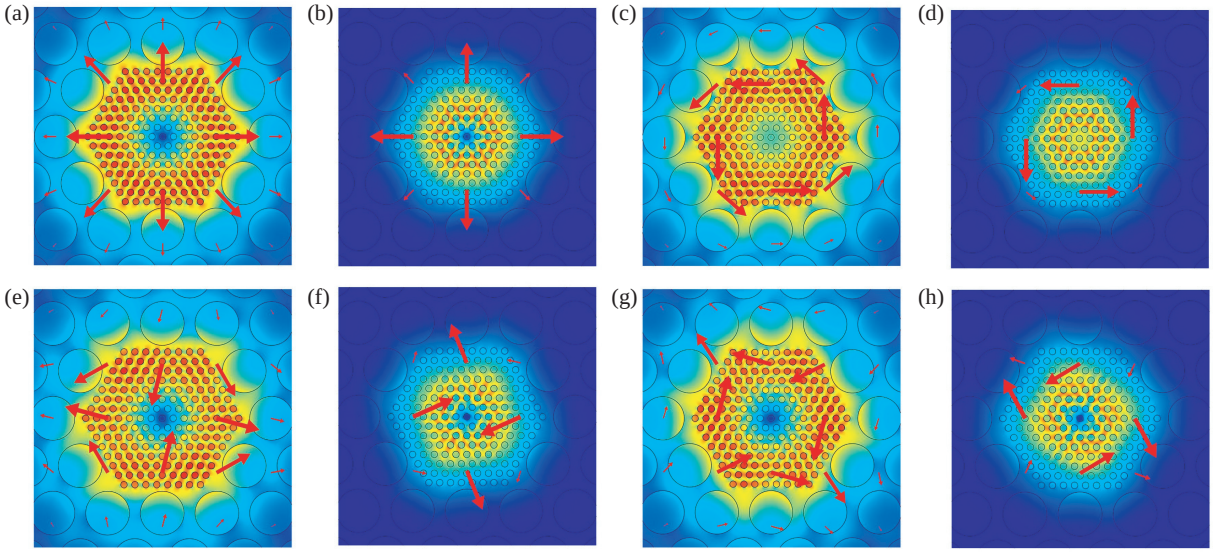


FIGURE 4. (a)–(b) TM_{01} (radially polarized mode), (c)–(d) TE_{01} (azimuthally polarized mode), (e)–(f) HE_{21}^{even} (hybrid-even mode), (g)–(h) HE_{21}^{odd} (hybrid-odd mode) for normal and GRIN type PCF.

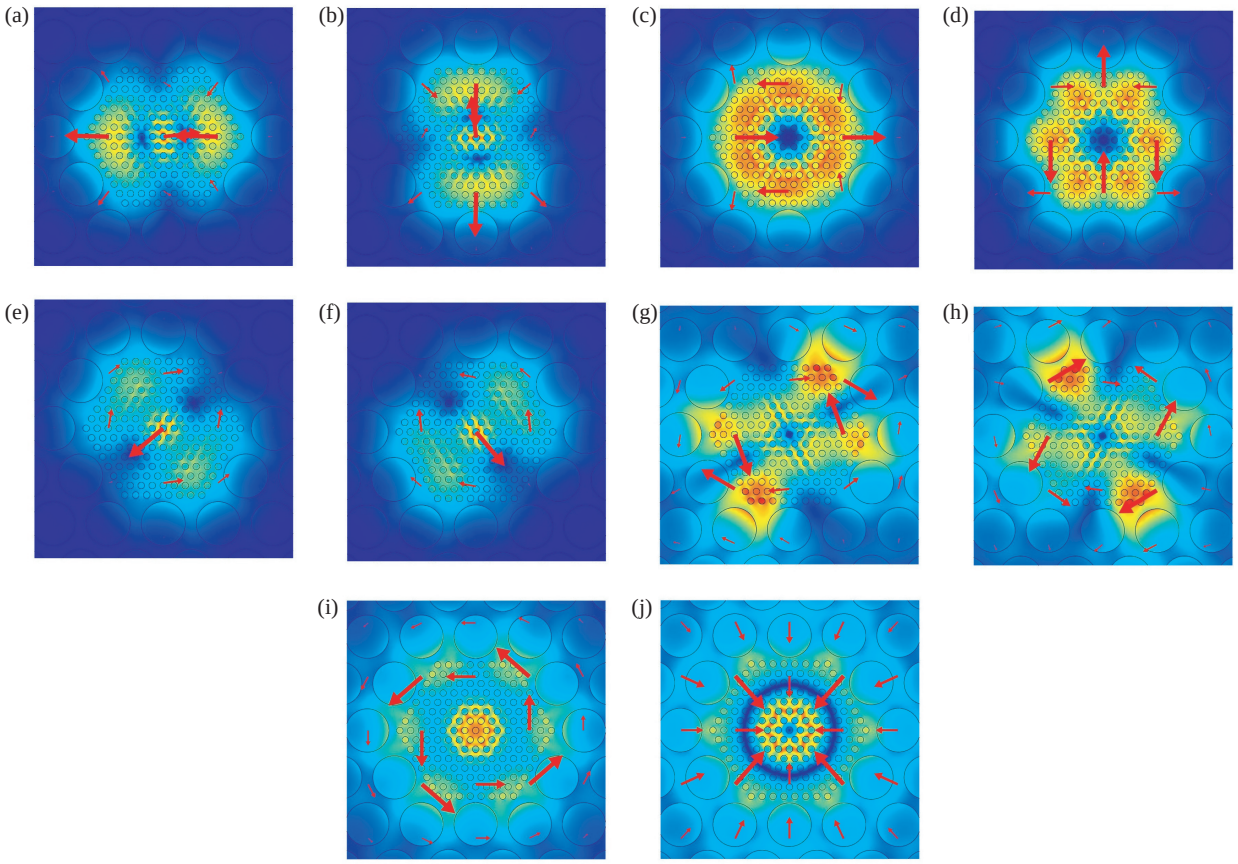


FIGURE 5. (a) HE_{31}^{even}, (b) HE_{31}^{odd}, (c) EH_{11}^{even}, (d) EH_{11}^{odd}, (e) HE_{12}^{x}, (f) HE_{12}^{y}, (g) HE_{22}^{even}, (h) HE_{22}^{odd}, (i) TE_{02}, (j) TM_{02} mode at 0.2 THz for GRIN profile PCF.

proceeds to travel in the same direction without any reflection delivering maximum transmission at the receiving end for the GRIN PCF. A generalization of group velocity is achievable by considering the evident speed of the maximum peak (marked as a dotted line in the subsequent figure) in the wave packet. It can be observed that the wave packet moves rightward with a positive power propagation for the realized GRIN PCF. The GRIN PCF gives better matching between the input source and GRIN

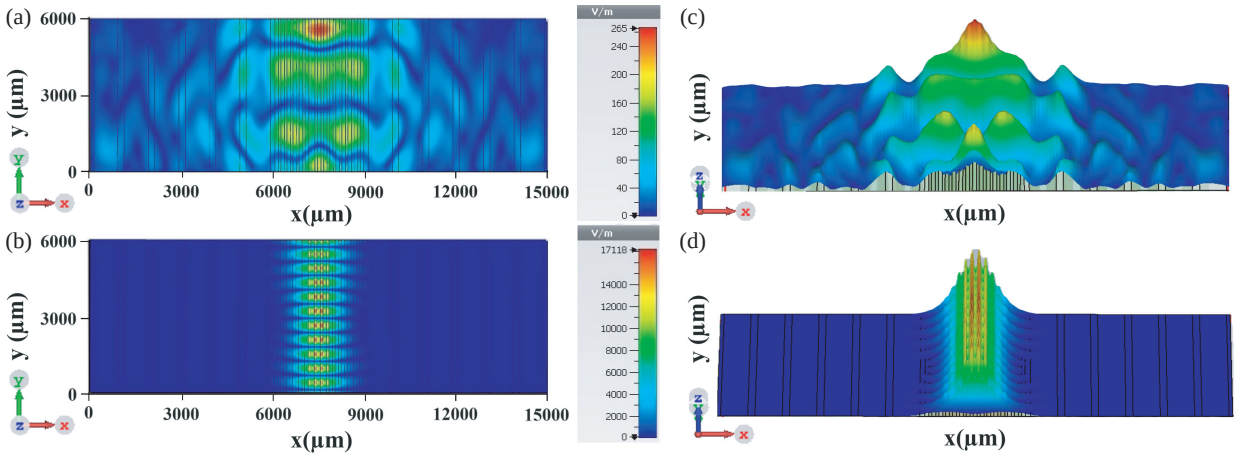


FIGURE 6. Propagation of EM wave at 0.2 THz, (a) normal type PCF, (b) GRIN type PCF, (c) normal PCF (3-D view), and (d) GRIN PCF (3-D view).

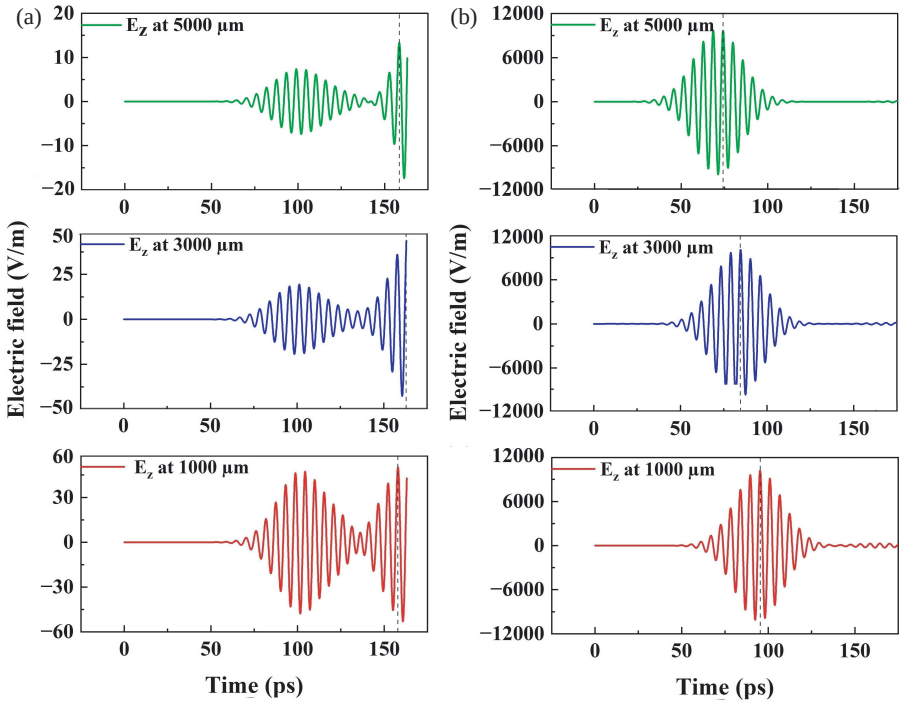


FIGURE 7. Dispersion characteristics, (a) normal type PCF, (b) GRIN type PCF.

PCF due to the graded index profile so that the reflection at the input port is minimal compared to the normal PCF case. The better matching in GRIN PCF is attributed to a two-step localization process where the execution of the GRIN profile supports sub-wavelength confinement, and it gives a high-quality factor of the GRIN PCF mode corresponding to the enhancement in the localized field.

4. GUIDING CHARACTERISTICS OF THE PROPOSED GRIN PCF

The guiding properties of the PCF such as quality factor, power fraction, and confinement loss are determined. The quality factor is calculated using the equation [43],

$$Q = f_r/\Delta f \tag{2}$$

where f_r is the resonant frequency, and Δf is the full-width at half-maximum (FWHM). To compute the quality factor numerically, several data points are essential. Accordingly, when the data points are increased from 51 to 1001, the quality factor is nearly repeated for a few cases, and it is sufficiently converged for 701 points. From Figs. 8(a)–(b), Q value is found as 2.4598×10^8 (where $f_r = 0.206263$ THz and FWHM = 8.3853×10^{-10} THz) for HE_{11} mode with normal index profile and 2.2849×10^9 (where $f_r = 0.1999966$ THz and FWHM = 8.7530×10^{-11} THz) for HE_{11} mode with GRIN profile which is 10 times greater than that of the conventional case. Hence,

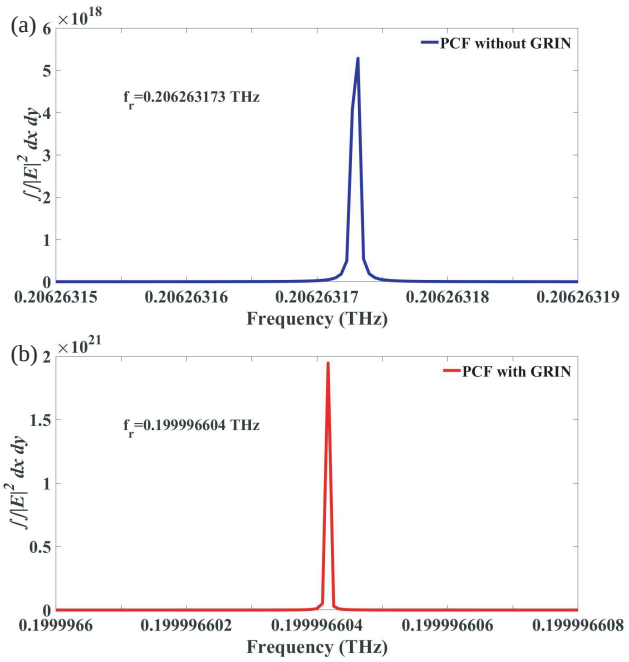


FIGURE 8. Estimation of quality factor, (a) normal PCF, (b) GRIN PCF.

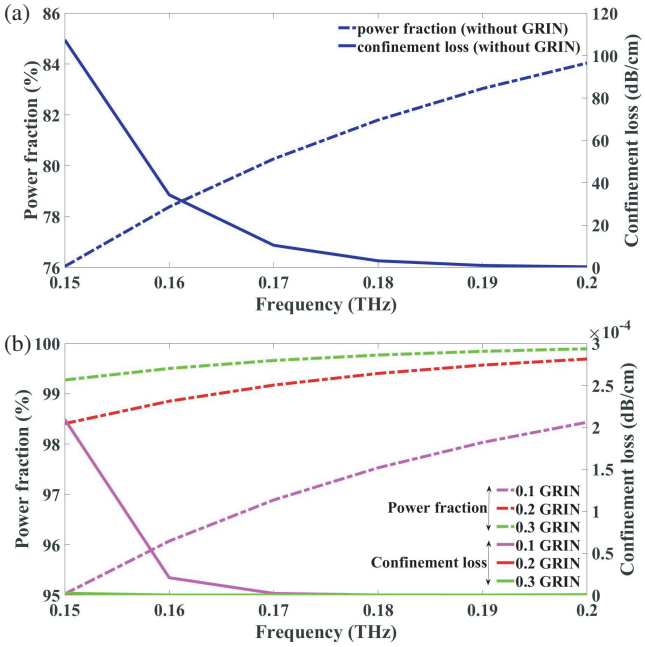


FIGURE 9. The values of power fraction and confinement loss for different frequencies, (a) HE_{11} mode without GRIN, (b) HE_{11} mode with GRIN.

this higher Q value leads to very narrow and intense in-plane confinement in the sub-wavelength range.

The overall power transmitting through the PCF core is termed as power fraction [44],

$$PF = \frac{\int_{core} \mathrm{Re}\,(E_x H_y - E_y H_x)\mathrm{d}x\mathrm{d}y}{\int_{overall} \mathrm{Re}\,(E_x H_y - E_y H_x)\mathrm{d}x\mathrm{d}y} \times 100\% \qquad (3)$$

where E_x, E_y, H_x, and H_y are the x- and y-components of the electric field and magnetic fields, respectively. The PF is evaluated as 84.04% for normal index profile PCF and 99.69% for GRIN profile PCF at 0.2 THz implying the maximum propagation of HE_{11} mode along the core with the application of triangular GRIN profile. The leakage of light outside the interface of the core and cladding corresponds to the confinement loss given as [45],

$$\alpha_{CL}\,(\mathrm{dB/cm}) = 8.686\frac{2\pi f}{c}\mathrm{Im}\,(n_{eff}) \qquad (4)$$

where $\mathrm{Im}(n_{eff})$ is the imaginary part of the effective mode index, c the speed of light in vacuum, and f the frequency of the incident light. At 0.2 THz, α_{CL} is calculated as 0.31 dB/cm for PCF without GRIN and 0.341×10^{-7} dB/cm for PCF with GRIN. This reveals lower confinement loss owed to GRIN profile indicating maximum field localization in the porous core rather than cladding of the PCF.

An optimization is executed based on the difference in GRIN between the adjacent hole rings of the porous core. Here, the profile with refractive index difference (Δn) from 0.1 to 0.5 is taken into consideration. Among the refractive index differences, the light confinement is maximum for 0.5 index change and minimum for 0.1 index change. The choice of gradient index results in unique confinement modes with varying quality factors. The field confinement is maximum for all GRIN cases at 0.2 THz, and the Q value is obtained at this range only for 0.2 GRIN difference as shown in Table 1. Hence, 0.2 GRIN is considered as the optimum value even though the power fraction obtained as 99.975% is slightly higher for 0.5 GRIN. Due to prolonged computation of 0.4 and 0.5 GRIN cases, the power fraction and confinement loss values are reported for 0.1 to 0.3 GRIN from 0.15 THz to 0.2 THz.

TABLE 1. The values of the quality factor for GRIN (Δn) change from 0.1 to 0.5.

GRIN-Refractive index change (Δn)	Resonant frequency (THz)	Quality factor
0.1	0.179025	4.4473×10^8
0.2	0.1999966	2.2849×10^9
0.3	0.156807	3.9124×10^9
0.4	0.168131	6.5787×10^9
0.5	0.170921	2.1286×10^{10}

Figure 9 shows the attained values of power fraction and confinement loss from 0.15 THz to 0.2 THz for normal PCF (Fig. 9(a)) and GRIN PCF with three distinct cases (Fig. 9(b)). When the energy loss is included in the layers of the PCF (the imaginary part of the dielectric permittivity is considered in the calculation), the medium becomes lossy, and the effective mode index becomes imaginary indicating an increase in the confinement loss from 0.341×10^{-7} dB/cm to 1.96×10^6 dB/cm at 0.2 THz for a gradient index change of 0.2. Even if the con-

TABLE 2. Comparison of the proposed GRIN porous core PCF with previous works.

Gradient features	Lattice type	Index profile	Wavelength (or) Frequency	Main Functionality	References
graded-index clad	hexagonal	Parabolic	1550 nm	collimator	[21]
graded-index clad	rectangular	Triangular	1.55 µm	slow-light generation	[22]
graded-index clad	hybrid	-	2.8 µm	supercontinuum generation	[23]
graded-index clad	circular	Parabolic	1.55 µm	transmission of OAM modes	[24]
graded-index clad	hexagonal	Parabolic	1550 nm	optical delay line	[25]
GRIN porous core	hexagonal	Triangular	0.2 THz	sub-wavelength confinement in the sub-THz regime with OAM modes	Proposed work

finement loss increases, the mode pattern is not affected as the real part of the effective mode index remains the same after incorporating losses in the medium.

Additionally, the dependence of refractive index on temperature is found using the equation [46],

$$n_x = n_0 + \frac{dn}{dT}(T - T_0) \tag{5}$$

where n_x is the temperature-dependent refractive index, n_0 the refractive index at room temperature, $\frac{dn}{dT}$ the thermo-optic coefficient, T the absolute temperature, and T_0 the room temperature. There are no significant changes in the mode confinement when the linear temperature dependence of the refractive index is considered. Thus, the proposed fiber has good thermal stability as the linear variation of a temperature-dependent refractive index does not alter the mode confinement and mode frequency drastically in the range of room temperature to 210°C.

The propagation of the field can be progressive with high power fraction, low thermal stability, and low confinement loss through this optimization. This work regards the optimum condition with the refractive index change of 0.2 for the GRIN Profile given the quality of the propagating wave in that profile at 0.2 THz. A comparison is made among the previously published works on graded-index PCF as shown in Table 2. Hitherto, the published works involve graded-index in the cladding of the PCF whereas the proposed work implies GRIN in the porous core of the PCF which becomes challenging for sub-wavelength field confinement in the THz regime. In addition, the triangular index profile created in the hexagonal lattice is easy to fabricate compared to the parabolic index profile. Mainly in the proposed GRIN porous core PCF, 0.2 THz plays a vital role in sub-wavelength biomedical imaging applications.

5. CONCLUSION

The GRIN PCF realized in this work manipulates the light with the help of PhC arrays for both core and cladding, where the core is designed with gradient PhC. The presented results open up a new approach to finely tune the resonant modes to the sub-wavelength scale. The confined field in the sub-wavelength level propagates through a triangular GRIN profile with superior intensity compared to the conventional profile. In the numerical analysis, a high-quality factor of 2.2849×10^9 in addition to a higher power fraction of 99.69% and lower confinement loss of 0.341×10^{-7} dB/cm has been accomplished with notable dispersion characteristics. Also, this particular porous core structure with GRIN profile is utilized to generate radially and azimuthally polarized modes along with additional OAM modes in the THz regime. As a result, the mode confinement and propagation assisted by the proposed GRIN PCF suggest the possibility of employing a sub-THz regime for communication, sensing and imaging applications. The numerically investigated PCF might be experimentally demonstrated using recent fabrication techniques.

ACKNOWLEDGEMENT

We thank Barkathulla Asrafali, College of Physics and Optoelectronics Engineering, Shenzhen University for computational assistance.

REFERENCES

[1] Aly, A. H. and F. A. Sayed, "THz cutoff frequency and multifunction $Ti_2Ba_2Ca_2Cu_3O_{10}$/GaAs photonic bandgap materials," *International Journal of Modern Physics B*, Vol. 34, No. 10, 2050091, 2020.

[2] Cordier, M., A. Orieux, R. Gabet, T. Harlé, N. Dubreuil, E. Diamanti, P. Delaye, and I. Zaquine, "Raman-tailored photonic crystal fiber for telecom band photon-pair generation," *Optics Letters*, Vol. 42, No. 13, 2583–2586, 2017.

[3] Ravi, A., M. Beck, D. F. Phillips, A. Bartels, D. Sasselov, A. Szentgyorgyi, and R. L. Walsworth, "Visible-spanning flat supercontinuum for astronomical applications," *Journal of Lightwave Technology*, Vol. 36, No. 22, 5309–5315, 2018.

[4] Xie, S., A. Sharma, R. Zeltner, and P. Russell, "On-the-fly particle metrology in hollow-core photonic crystal fiber," in *Asia Communications and Photonics Conference*, S4G–2, Beijing, China, 2020.

[5] Eravuchira, P. J., M. Banchelli, C. D'Andrea, M. D. Angelis, P. Matteini, and I. Gannot, "Hollow core photonic crystal fiber-assisted raman spectroscopy as a tool for the detection of alzheimer's disease biomarkers," *Journal of Biomedical Optics*, Vol. 25, No. 7, 077 001–077 001, 2020.

[6] Soltanian, M. R. K., I. S. Amiri, S. E. Alavi, and H. Ahmad, "Dual-wavelength erbium-doped fiber laser to generate terahertz

radiation using photonic crystal fiber," *Journal of Lightwave Technology*, Vol. 33, No. 24, 5038–5046, 2015.

[7] Zhang, L., S. Yang, X. Wang, D. Gou, W. Chen, W. Luo, H. Chen, M. Chen, and S. Xie, "Photonic crystal fiber based wavelength-tunable optical parametric amplifier and picosecond pulse generation," *IEEE Photonics Journal*, Vol. 6, No. 5, 1–8, 2014.

[8] Amiri, I. S., B. K. Paul, K. Ahmed, A. H. Aly, R. Zakaria, P. Yupapin, and D. Vigneswaran, "Tri-core photonic crystal fiber based refractive index dual sensor for salinity and temperature detection," *Microwave and Optical Technology Letters*, Vol. 61, No. 3, 847–852, 2019.

[9] Yasli, A., H. Ademgil, S. Haxha, and A. Aggoun, "Multi-channel photonic crystal fiber based surface plasmon resonance sensor for multi-analyte sensing," *IEEE Photonics Journal*, Vol. 12, No. 1, 1–15, 2020.

[10] Paul, B. K., K. Ahmed, V. Dhasarathan, F. A. Al-Zahrani, M. N. Aktar, M. S. Uddin, and A. H. Aly, "Investigation of gas sensor based on differential optical absorption spectroscopy using photonic crystal fiber," *Alexandria Engineering Journal*, Vol. 59, No. 6, 5045–5052, 2020.

[11] Rani, K. R., K. Ravichandran, and N. Yogesh, "Group velocity dispersion in terahertz hollow-core hexagonal photonic crystal fiber," in *2019 Workshop on Recent Advances in Photonics (WRAP)*, 1–3, Guwahati, India, 2019.

[12] Rani, K. R. and K. Chitra, "Design and analysis of low loss solid-core hexagonal photonic crystal fiber for applications in terahertz regime," *Journal of Physics: Conference Series*, Vol. 2426, No. 1, 012019, 2023.

[13] Malek, C., A. H. Aly, S. Alamri, and W. Sabra, "Tunable PBGs with a cutoff frequency feature in Fibonacci quasi-periodic designs containing a superconductor material at THz region," *Physica Scripta*, Vol. 96, No. 10, 105501, 2021.

[14] Yogesh, N. and V. Subramanian, "Spatial beam compression and effective beam injection using triangular gradient index profile photonic crystals," *Progress In Electromagnetics Research*, Vol. 129, 51–67, 2012.

[15] Shi, P., K. Huang, and Y.-P. Li, "Subwavelength imaging by a graded-index photonic-crystal flat lens in a honeycomb lattice," *Journal of the Optical Society of America A*, Vol. 28, No. 10, 2171–2175, 2011.

[16] Turduev, M., I. H. Giden, and H. Kurt, "Design of flat lens-like graded index medium by photonic crystals: Exploring both low and high frequency regimes," *Optics Communications*, Vol. 339, 22–33, 2015.

[17] Kurt, H. and D. S. Citrin, "A novel optical coupler design with graded-index photonic crystals," *IEEE Photonics Technology Letters*, Vol. 19, No. 19, 1532–1534, 2007.

[18] Oner, B. B., M. Turduev, I. H. Giden, and H. Kurt, "Efficient mode converter design using asymmetric graded index photonic structures," *Optics Letters*, Vol. 38, No. 2, 220–222, 2013.

[19] Dash, D. and J. Saini, "Sensitivity analysis of step index and graded index one dimensional cavity-based cholesterol sensor," *Optical and Quantum Electronics*, Vol. 55, No. 4, 349, 2023.

[20] Wang, H.-W. and L.-W. Chen, "High transmission efficiency of arbitrary waveguide bends formed by graded index photonic crystals," *Journal of the Optical Society of America B*, Vol. 28, No. 9, 2098–2104, 2011.

[21] Wakabayashi, M., H. Yokota, and Y. Imai, "Optical coupling characteristics of graded-index type photonic crystal fiber collimator depending on air hole diameter ratio to pitch," *Optical Review*, Vol. 26, No. 6, 590–596, 2019.

[22] Yadav, S., A. Kumar, T. S. Saini, and R. K. Sinha, "SBS based slow-light generation in rectangular lattice graded-index photonic crystal fiber: Design and analysis," *Optik*, Vol. 132, 164–170, 2017.

[23] Chaitanya, A. G. N., T. S. Saini, A. Kumar, and R. K. Sinha, "Ultra broadband mid-IR supercontinuum generation in $Ge_{11.5}As_{24}Se_{64.5}$ based chalcogenide graded-index photonic crystal fiber: Design and analysis," *Applied Optics*, Vol. 55, No. 36, 10 138–10 145, 2016.

[24] Zhang, X., Q. Ma, W. He, W. Hong, and Z. Deng, "Graded ring-core photonic crystal fiber for the transmission of OAM modes with high mode purity and quality in C + L bands," *Optics Communications*, Vol. 520, 128486, 2022.

[25] Higuchi, K., H. Yokota, K. Yoneya, and Y. Imai, "Connection loss reduction in variable optical delay line by using graded-index type photonic crystal fiber," *IEEJ Transactions on Electrical and Electronic Engineering*, Vol. 13, No. 5, 742–747, 2018.

[26] Cluzel, B., D. Gérard, E. Picard, T. Charvolin, F. De Fornel, and E. Hadji, "Subwavelength imaging of field confinement in a waveguide-integrated photonic crystal cavity," *Journal of Applied Physics*, Vol. 98, No. 8, 086109, 2005.

[27] Louvion, N., A. Rahmani, C. Seassal, S. Callard, D. Gérard, and F. De Fornel, "Near-field observation of subwavelength confinement of photoluminescence by a photonic crystal microcavity," *Optics Letters*, Vol. 31, No. 14, 2160–2162, 2006.

[28] Zheltikov, A. M., "Subwavelength confinement of electromagnetic field by guided modes of dielectric micro-and nanowaveguides," *JETP Letters*, Vol. 91, 378–381, 2010.

[29] Vignolini, S., F. Intonti, F. Riboli, M. Zani, A. Vinattieri, D. S. Wiersma, M. Colocci, L. Balet, L. Li, M. Francardi, A. Gerardino, A. Fiore, and M. Gurioli, "Sub-wavelength probing and modification of photonic crystal nano-cavities," *Photonics and Nanostructures — Fundamentals and Applications*, Vol. 8, No. 2, 78–85, 2010.

[30] Hu, S., M. Khater, R. Salas-Montiel, E. Kratschmer, S. Engelmann, W. M. J. Green, and S. M. Weiss, "Experimental realization of deep-subwavelength confinement in dielectric optical resonators," *Science Advances*, Vol. 4, No. 8, eaat2355, 2018.

[31] Yu, X., J.-Y. Kim, M. Fujita, and T. Nagatsuma, "Efficient mode converter to deep-subwavelength region with photonic-crystal waveguide platform for terahertz applications," *Optics Express*, Vol. 27, No. 20, 28 707–28 721, 2019.

[32] Kong, W., Y. Sun, R. Meng, and X. Ni, "Low-loss light guiding at the subwavelength scale in a nanowire-loaded hybrid bloch-surface-polariton waveguide," *IEEE Access*, Vol. 8, 191 795–191 802, 2020.

[33] Arnold, K. P., S. I. Halimi, J. A. Allen, S. Hu, and S. M. Weiss, "Photonic crystals with split ring unit cells for subwavelength light confinement," *Optics Letters*, Vol. 47, No. 3, 661–664, 2022.

[34] Qin, Y., C. Ma, Y. Lian, L. Huang, Y. Yuan, M. Sha, X. Ye, and K. Zheng, "Mid-infrared deep subwavelength confinement in graphene plasmonic waveguides," *Diamond and Related Materials*, Vol. 144, 111046, 2024.

[35] Oulton, R. F., V. J. Sorger, D. A. Genov, D. F. P. Pile, and X. Zhang, "A hybrid plasmonic waveguide for subwavelength confinement and long-range propagation," *Nature Photonics*, Vol. 2, No. 8, 496–500, 2008.

[36] Kabir, M. A., M. M. Hassan, K. Ahmed, M. S. M. Rajan, A. H. Aly, M. N. Hossain, and B. K. Paul, "Novel spider web photonic crystal fiber for robust mode transmission applications with supporting orbital angular momentum transmission property," *Optical and Quantum Electronics*, Vol. 52, 1–17, 2020.

[37] Ung, B., P. Vaity, L. Wang, Y. Messaddeq, L. A. Rusch, and S. LaRochelle, "Few-mode fiber with inverse-parabolic graded-index profile for transmission of OAM-carrying modes," *Optics Express*, Vol. 22, No. 15, 18 044–18 055, 2014.

[38] Nandam, A. and W. Shin, "Spiral photonic crystal fiber structure for supporting orbital angular momentum modes," *Optik*, Vol. 169, 361–367, 2018.

[39] Sharma, M., P. Pradhan, and B. Ung, "Endlessly mono-radial annular core photonic crystal fiber for the broadband transmission and supercontinuum generation of vortex beams," *Scientific Reports*, Vol. 9, No. 1, 2488, 2019.

[40] Zhang, Z., J. Lu, T. Liu, J. Gan, X. Heng, M. Wu, F. Li, and Z. Yang, "Azimuthally and radially polarized orbital angular momentum modes in valley topological photonic crystal fiber," *Nanophotonics*, Vol. 10, No. 16, 4067–4074, 2021.

[41] Zhang, X., M. Chang, N. Chen, X. Liu, J. Zhang, J. Du, and X. Ding, "Ultra-broadband mid-infrared TE01 vector mode selector based on ring-core few-mode photonic crystal fiber," *Optical Fiber Technology*, Vol. 70, 102859, 2022.

[42] Aly, A. H., S.-W. Ryu, H.-T. Hsu, and C.-J. Wu, "THz transmittance in one-dimensional superconducting nanomaterial-dielectric superlattice," *Materials Chemistry and Physics*, Vol. 113, No. 1, 382–384, 2009.

[43] Mohammed, N. A., M. M. Hamed, A. A. M. Khalaf, A. Alsayyari, and S. El-Rabaie, "High-sensitivity ultra-quality factor and remarkable compact blood components biomedical sensor based on nanocavity coupled photonic crystal," *Results in Physics*, Vol. 14, 102478, 2019.

[44] Ahmed, K., F. Ahmed, S. Roy, B. K. Paul, M. N. Aktar, D. Vigneswaran, and M. S. Islam, "Refractive index-based blood components sensing in terahertz spectrum," *IEEE Sensors Journal*, Vol. 19, No. 9, 3368–3375, 2019.

[45] He, T. and B. Wu, "Low confinement loss photonic crystal fibre capable of supporting 54 orbital angular momentum modes," *Journal of Modern Optics*, Vol. 67, No. 6, 556–562, 2020.

[46] Wang, M., Y. Lu, C. Hao, X. Yang, and J. Yao, "Simulation analysis of a temperature sensor based on photonic crystal fiber filled with different shapes of nanowires," *Optik*, Vol. 126, No. 23, 3687–3691, 2015.